

## Rapid microwave-assisted fabrication of 3D cauliflower-like NiCo<sub>2</sub>S<sub>4</sub> architectures for asymmetric supercapacitors

Yanling Xiao,<sup>a</sup> Ying Lei,<sup>b</sup> Baozhan Zheng,<sup>a</sup> Li Gu,<sup>a</sup> Yanyan Wang<sup>b</sup> and Dan Xiao<sup>\*ab</sup>

<sup>a</sup>College of Chemistry

<sup>b</sup>College of Chemical Engineering, Sichuan University, 29 Wangjiang Road, Chengdu 610064, China.

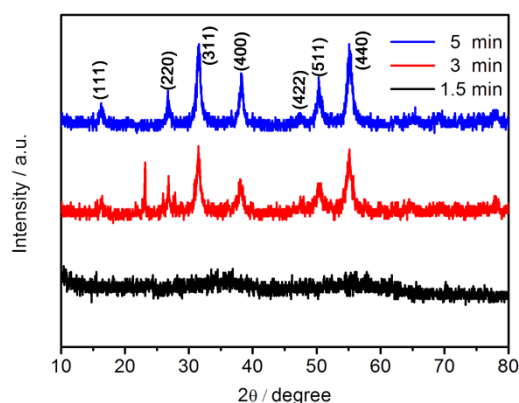
\*Corresponding author: xiaodan@scu.edu.cn (Dan Xiao);

### Preparation of Activated Carbon (AC):

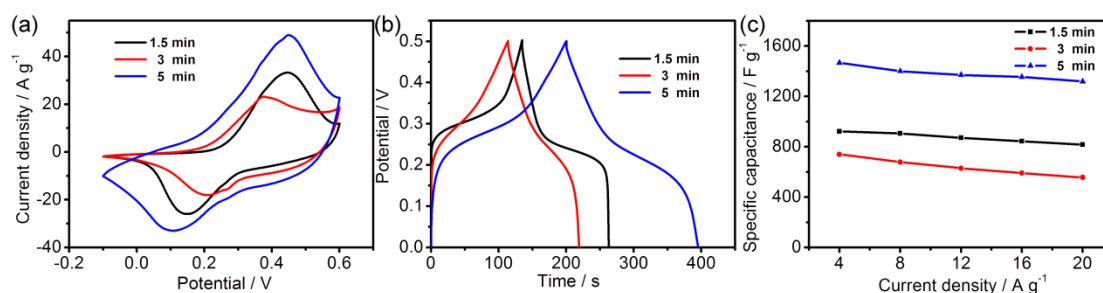
In a typical experiment, 10.0 g of phenol formaldehyde resin was dissolved in 200 mL of 1 M KOH solution. Then the mixtures were stirring for 12 h at room temperature. After that, the precipitates were obtained by filtration. The precipitates were dried in a vacuum at 60 °C overnight and then calcinated in Ar at 750 °C for 3 h. After the reaction mixtures cooling down to room temperature, the precipitates were washed with 1 M HCl and distilled water for several times, respectively. The final products were dried in vacuum at 105 °C overnight.

**Table S1.** The relative content of Co<sup>2+</sup> and Co<sup>3+</sup> as well as Ni<sup>2+</sup> and Ni<sup>3+</sup> in NiCo<sub>2</sub>S<sub>4</sub>.

State of Co	Co <sup>2+</sup>	Co <sup>3+</sup>	State of Ni	Ni <sup>2+</sup>	Ni <sup>3+</sup>
Amount (%)	32.00 ± 1.23	68.00 ± 1.23	Amount (%)	64.90 ± 1.89	35.1 ± 1.89

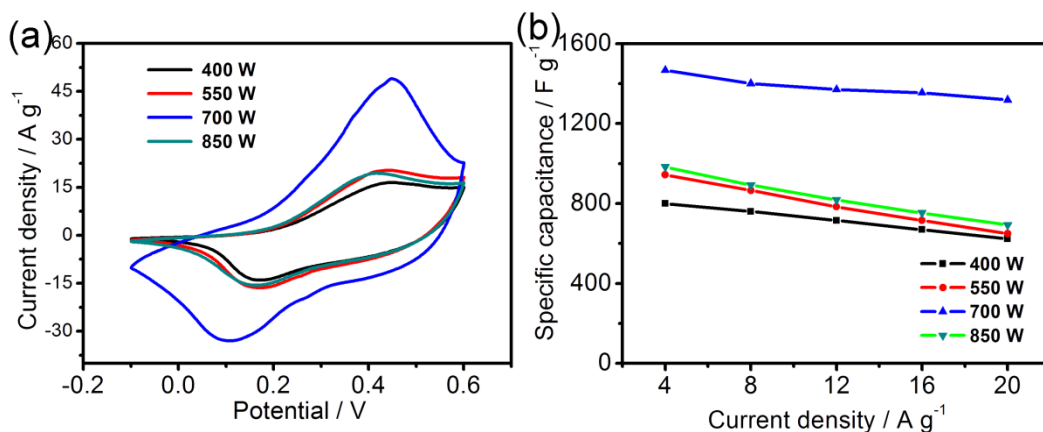


**Fig. S1** XRD patterns of the samples collected at the different reaction time (1.5 min, 3 min, 5 min).



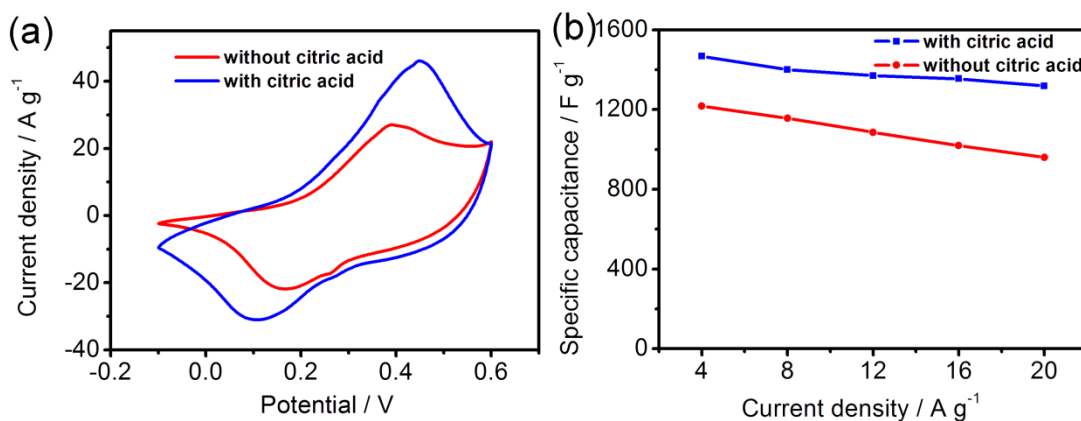
**Fig. S2** (a) CV curves ( $20 \text{ mV s}^{-1}$ ), (b) galvanostatic charge-discharge curves ( $4 \text{ A g}^{-1}$ ) and (c) the corresponding capacitance values versus current densities of the samples collected at different reaction time (1.5 min, 3 min, 5 min).

Comparing the three CV curves, it can be observed that the CV integrated area of the samples collected at 5 min (Fig. S2a, blue curve) is the largest, which is probably ascribed to the high purity of  $\text{NiCo}_2\text{S}_4$  which has richer redox ability.<sup>1</sup> From the galvanostatic charge-discharge curves (Fig. S2b), the sample collected at 5 min also shows the longest discharge time, which is agreement with the CV result. In addition, the sample obtained at 5 min exhibits superior capacitance (Fig. S2c), indicating that capacitance performance could be partly affected by the purity and crystallinity of  $\text{NiCo}_2\text{S}_4$ .



**Fig. S3** (a) CV curves ( $20 \text{ mV s}^{-1}$ ) and (b) capacitance values at the different current densities of the samples collected at different reaction power (400 W, 550 W, 700 W, and 850 W).

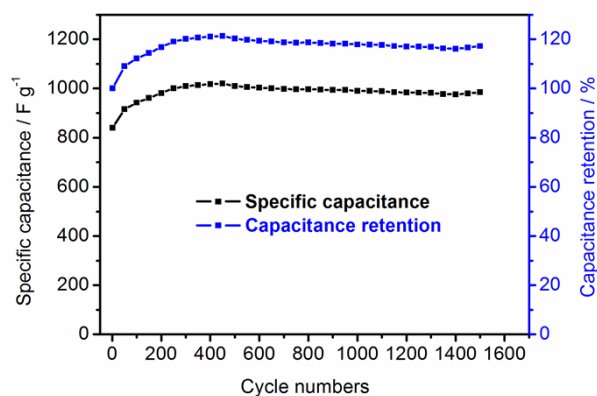
As shown in Fig. S3a, the CV integrated area of the samples prepared at 700 W is the largest. Moreover, the capacitances of the samples collected at the different reaction power were also conducted and the corresponding results are shown in Fig. S3b. Remarkably, the capacitance of the materials prepared at 700 W is the most prominent.



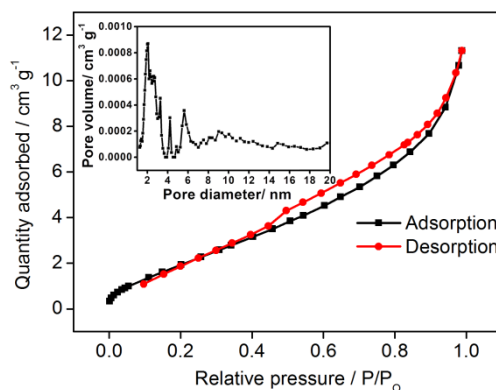
**Fig. S4** (a) CV curves ( $20 \text{ mV s}^{-1}$ ) and (b) capacitances at different current densities of the NiCo<sub>2</sub>S<sub>4</sub> materials obtained with and without citric acid.

From Fig. S4a, it is easily observed that the current density and the CV integrated area of the samples prepared with citric acid are much larger than the materials prepared without citric acid. Remarkably, the specific capacitance values of the materials prepared with citric acid are significantly higher than those of the samples

without citric acid (Fig. S4b). In fact, the purpose of adding citric acid in the reaction system is to control the reaction rate by the complexation of citric acid with metal ions.<sup>2</sup>

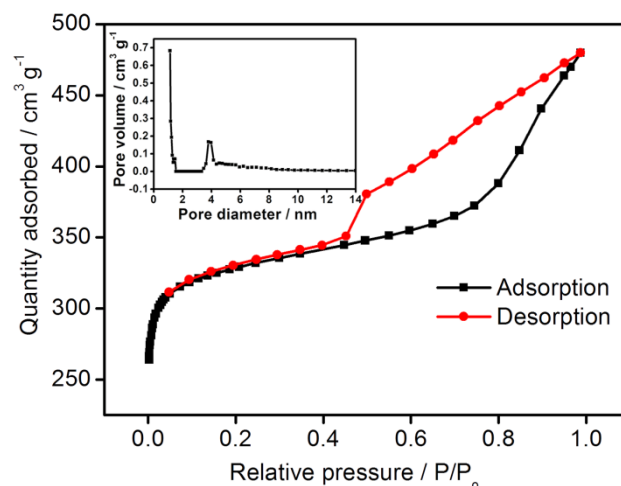


**Fig. S5** Specific capacitance and capacitance retention against cycle numbers at 30  $\text{mV s}^{-1}$  of the 3D cauliflower-like  $\text{NiCo}_2\text{S}_4$ -modified electrode.



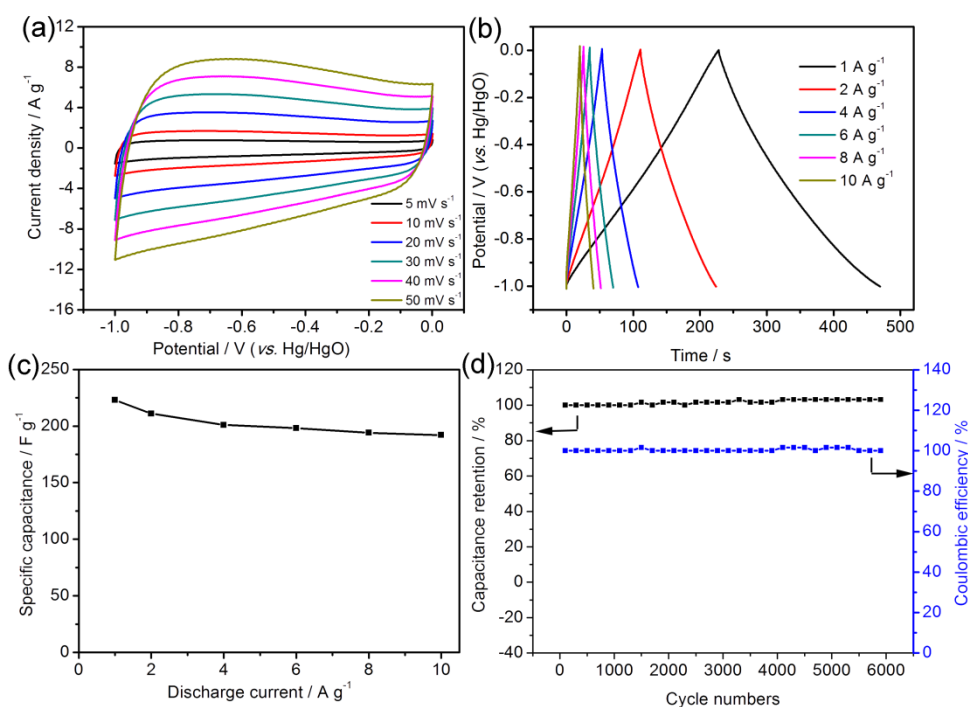
**Fig. S6**  $\text{N}_2$  adsorption-desorption isotherm and the inset presents pore size distribution of the prepared  $\text{NiCo}_2\text{S}_4$ .

Fig. S6 presents the  $\text{N}_2$  adsorption and desorption isotherm loop and the pore size distribution (PSD, inset) of the prepared  $\text{NiCo}_2\text{S}_4$  assessed by non-local density functional theory (NLDFT) method. The Brunauer-Emmett-Teller (BET) surface area of  $\text{NiCo}_2\text{S}_4$  is calculated to be  $8.32 \text{ m}^2 \text{ g}^{-1}$  and the average pore diameter is 2.1 nm.



**Fig. S7** N<sub>2</sub> adsorption-desorption isotherm and the inset presents pore size distribution of the prepared AC.

Fig. S7 presents the N<sub>2</sub> adsorption-desorption isotherm and the PSD (inset) of the prepared AC. There is a distinct hysteresis loop (0.4-1.0  $P/P_0$ ) and a steep uptake ( $P/P_0 < 0.02$ ) appeared in the N<sub>2</sub> adsorption-desorption isotherm, indicating that the as-prepared AC possesses some mesopores and micropores.<sup>3,4</sup> Based on BET analysis, its specific surface area is 1279 m<sup>2</sup> g<sup>-1</sup>. The PSD of the prepared AC measured by the Barrett-Joyner-Halenda (BJH) method also confirm the existence of mesopores and micropores in the materials. The average pore diameter and pore volume of the AC samples are 2.9 nm and 0.7 cm<sup>3</sup> g<sup>-1</sup>, respectively.



**Fig. S8** (a) CV curves with various scan rates and (b) galvanostatic charge-discharge curves of the AC-modified electrode in 6 M KOH. (c) The corresponding capacitance values. (d) Cycle stability and coulombic efficiency of the AC-modified electrode at 10 A g<sup>-1</sup>.

The electrochemical capacitive behaviours of AC-modified electrode were tested in a three-electrode system. Fig. S8a shows typical CV curves of AC-modified electrode with various scan rates (5, 10, 20, 30, 40, 50 mV s<sup>-1</sup>) at the potential window of -1.0~0 V (vs. Hg/HgO) in 6.0 M KOH. Each of the curves presents ideal rectangular shape indicating that a electrical double layer has formed on the surface of the AC-modified electrode. Fig. S8b presents the galvanostatic charge-discharge curves of AC-modified electrode at various current densities between -1.0 and 0 V. The triangular shapes of the charge-discharge curves show mainly the characteristic of EDLC, which is consistent with the CV tests. Based on the charge-discharge curves, the specific capacitances of the materials are calculated and the corresponding results are shown in Fig. S8c. The AC materials exhibit a maximum capacitance of 223 F g<sup>-1</sup> at 1 A g<sup>-1</sup>. At a high density of 10 A g<sup>-1</sup> the capacitance value still remains to be 86% of that at 1 Ag<sup>-1</sup>, revealing remarkable rate capability.

Consecutive galvanostatic charge-discharge was investigated at  $10 \text{ A g}^{-1}$  between -1 and 0 V for 6000 repetitive cycles. As shown in Fig. S8d, the specific capacitance of the AC-modified electrode shows no decrease even after 6000 cycles which indicates outstanding stability. In addition, the coulombic efficiency of the AC-modified electrode remains above 99%, suggesting the AC materials is highly reversible.

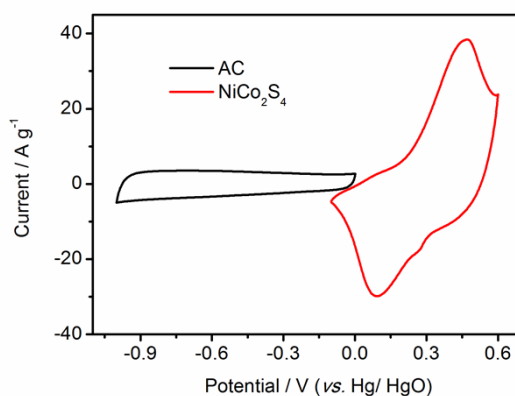


**Fig. S9** CV curves of NiCo<sub>2</sub>S<sub>4</sub> and AC electrodes performed in a three-electrode system in 6 M KOH at  $20 \text{ mV s}^{-1}$ .

Fig. S9 shows the CV curves of NiCo<sub>2</sub>S<sub>4</sub>-modified electrode and AC-modified electrode. The potential windows of NiCo<sub>2</sub>S<sub>4</sub>-modified electrode and AC-modified electrode are  $-0.1\sim 0.6 \text{ V}$  and  $-1.0\sim 0 \text{ V}$  (vs. Hg/HgO), respectively (Fig. S9). The NiCo<sub>2</sub>S<sub>4</sub>-modified electrode and AC-modified electrode were measured at different potentials and all demonstrate stable electrochemical performance. To obtain a capacitor operating in a 1.6 V potential window, the NiCo<sub>2</sub>S<sub>4</sub>-modified electrode and the AC-modified electrode are necessary to work at the potential windows of  $0\sim 0.6 \text{ V}$  and  $-1.0\sim 0 \text{ V}$ , respectively, which can ensure good properties of the two materials during cycle process.<sup>5</sup>

**Table S2.** The specific capacitance and capacitance retention of the cauliflower-like NiCo<sub>2</sub>S<sub>4</sub> prepared in this work and other materials in literatures.

Materials	Current density (A g <sup>-1</sup> )	Capacitance (F g <sup>-1</sup> )	Capacitance retention (%)	Reference
NiCo <sub>2</sub> S <sub>4</sub> nanosheets on graphene	3-20	1451-760	52.4	13
Urchin-like NiCo <sub>2</sub> S <sub>4</sub>	1-20 1-50	1149-888 1149-761	77.3 66.2	17
NiCo <sub>2</sub> S <sub>4</sub> nanotubes on foam	2-32	783-576	73.6	18
NiCo <sub>2</sub> S <sub>4</sub> Porous nanotubes	1-5	933-550	58.9	19
CoNi <sub>2</sub> S <sub>4</sub> nanoparticles	1-5	1169-702	60.1	32
NiCo <sub>2</sub> O <sub>4</sub> Nanowires	1-20	722-568	78.7	11
Flower-like NiCo <sub>2</sub> O <sub>4</sub> Microspheres	2-20	1444-1048	72.6	33
Nickel sulfide hollow spheres	4.08-8.16	927-618	66.7	34
CoS <sub>2</sub> ellipsoids	1-10	980-224	22.9	35
Cauliflower-like NiCo <sub>2</sub> S <sub>4</sub>	1-5	1471-1432	97.3	This work
	1-10	1471-1372	93.3	
	1-20	1471-1272	86.5	
	2-32	1470-1139	77.5	
	1-50	1471-940	63.9	

## References

1. H. C. Chen, J. J. Jiang, L. Zhang, H. Z. Wan, T. Qi and D. D. Xia, *Nanoscale*, 2013, **5**, 8879-8883.
2. F. L. Luo, J. Li, H. Y. Yuan and D. Xiao, *Electrochimi. Acta*, 2014, **123**, 183-189.
3. M. W. Xu, L. B. Kong, W. J. Zhou and H. L. Li, *J. Phys. Chem. C*, 2007, **111**, 19141-19147.
4. C. C. Yu, L. X. Zhang, J. L. Shi, J. J. Zhao, J. H. Gao and D. S. Yan, *Adv. Funct. Mater.*, 2008, **18**, 1544-1554.
5. P. C. Chen, G. Z. Shen, Y. Shi, H. T. Chen and C. W. Zhou, *ACS Nano*, 2010, **4**, 4403-4411.